Anisotropic Cation Exchange in PbSe/CdSe Core/Shell Nanocrystals of Different Geometry

ARTICLE *in* CHEMISTRY OF MATERIALS · DECEMBER 2011

Impact Factor: 8.35 · DOI: 10.1021/cm202796s

CHEMISTRY OF MATERIALS

Article

pubs.acs.org/cm

Anisotropic Cation Exchange in PbSe/CdSe Core/Shell Nanocrystals of Different Geometry

Marianna Casavola,*[,†] Marijn A. van Huis,[‡,§] Sara Bals,[‡] Karel Lambert,[⊥] Zeger Hens,[⊥] and Daniel Vanmaekelbergh*[,†]

[†]Condensed Matter and Interfaces, Debye Institute for Nanomaterials Science, Utrecht University, P.O. Box 80000, 3508 TA Utrecht, The Netherlands

[‡]EMAT-University of Antwerp, Groenenborgerlaan 171, B-2020 Antwerp, Belgium

[§]Kavli Institute of Nanoscience, Delft University of Technology, Lorentzweg 1, 2628 CJ Delft, The Netherlands

[⊥]Physics and Chemistry of Nanostructures, Ghent University, Krijgslaan 281-S12, B-9000 Ghent, Belgium

Supporting Information

ABSTRACT: We present a study of Cd^{2+}-for-Pb^{2+} exchange in PbSe nanocrystals (NCs) with cube, star, and rod shapes. Prolonged temperature-activated cation exchange results in PbSe/CdSe heterostructured nanocrystals (HNCs) that preserve their specific overall shape, whereas the PbSe core is strongly faceted with dominance of {111} facets. Hence, cation exchange proceeds while the Se anion lattice is preserved, and well-defined {111}/{111} PbSe/CdSe interfaces develop. Interestingly, by quenching the reaction at different stages of the cation exchange new structures have been isolated, such as core−shell nanorods, CdSe rods that contain one or two separated PbSe dots and fully zinc blende CdSe nanorods. The crystallographically anisotropic cation exchange has been characterized by a combined HRTEM/HAADF-STEM study of heterointerface evolution over reaction time and temperature. Strikingly, Pb and Cd are only intermixed at the PbSe/CdSe interface. We propose a plausible model for the cation exchange based on a layer-by-layer replacement of Pb^{2+} by Cd^{2+} enabled by a vacancy-assisted cation migration mechanism.

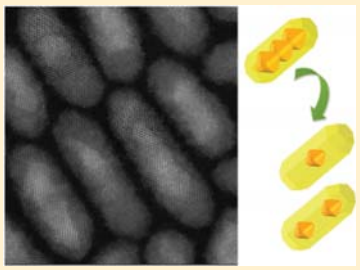

KEYWORDS: *core/shell nanocrystals, cation exchange, near-infrared-active nanocrystals, HAADF-STEM, PbSe/CdSe*

INTRODUCTION

Heterostructured nanocrystals (HNCs) based on semiconductors are a new brand of nanomaterials that are expected to have a great impact on the development of novel opto-electronic devices.[1,2] HNCs with core−shell geometry, consisting of semiconductor NCs epitaxially embedded in a second crystalline matrix, are a particularly advantageous system, because different band alignments are possible by controlling the material composition, the size of the two NC-sections and the coherence of the nanojunction.[2−4] Recently, nanostructured solids that contain PbX nanocrystals in a CdX matrix (where X = S, Se, Te) have been studied, in view of their promise for opto-electronic applications in the near-infrared.[5,6] It was found that rock salt (rs-) PbTe NCs embedded in a zinc blende (zb-) CdTe matrix can be obtained by thermally induced reconstruction of CdTe/PbTe films grown by MBE. The formation of cuboctahedron PbTe cores is energetically favorable at high temperature and a number of sharp PbTe/CdTe interfaces forms, because of the very low reciprocal miscibility of PbTe and CdTe[7] and to the matching of the lattice constants of the rs and zb crystallographic structures.[5,6] In these nanostructures atomic position and bond direction rearrange in a different way across the relevant interfaces depending on the termination of the polar facets involved.[5] The tendency toward the formation of directional bonds and long-range electrostatic interactions determine the atoms displacement at the interface.[5]

It was recently shown that colloidal PbX/CdX core/shell HNCs can be obtained starting from nearly spherical PbX cores using a Cd^{2+}-for-Pb^{2+} cationic exchange (CE) process.[8,9] The formation of a CdSe shell around the PbSe core results in colloidal systems with a higher photoluminescence quantum yield in the near-IR and long carrier lifetimes.[8,10] Colloidal PbX/CdX core/shell HNCs could form a cost-effective alternative to MBE-grown systems, with the additional advantage of a better processability and versatility. CE is an emerging chemical method that allows low-temperature formation of colloidal NCs and heterostructures, not achievable by other methods.[11−15] However, the mechanism and the parameters that are important to control the process are not completely understood. Questions that are not, or only partially answered are related to (i) whether selective adsorption of the cation precursors at specific crystallographic facets of the nanocolloid is important, (ii) whether ion-transport or the atomic rearrangements at the interface is a limiting factor, (iii)

Received: September 17, 2011
Revised: November 3, 2011
Published: November 17, 2011

in the case ion transport is a limiting factor, is ion-diffusion isotropic or determined by the crystallography of the system.

In this contribution we have studied Cd^{2+}-for-Pb^{2+} CE for PbSe NCs. Differently from other systems, Cd^{2+}-for-Pb^{2+} CE is a relatively slow process and HNCs obtained at intermediate stages can be easily isolated and studied by different techniques. CE was performed starting from PbSe NCs with different geometries, i.e., cubes (being the natural shape of rs-PbSe), octahedron-like stars, and nanorods (NRs). These specific shapes and the related surface facets hold a strict relation with the rs-PbSe lattice. This should allow us to study the crystallographic aspects of CE. We have monitored the proceeding CE for PbSe NCs with specific shapes by state-of-the-art HRTEM and HAADF-STEM sample studies. This structural study allowed us to investigate the temperature-dependence and the crystallographically anisotropic nature of the CE process in the PbSe/CdSe system. We should remark here that we achieved unseen HNC structures, such as CdSe rods that contain one or two PbSe dots and zb-CdSe rods.

EXPERIMENTAL SECTION

All syntheses were carried out in an air-free environment. PbSe NCs syntheses were carried out in a standard Schlenk line under nitrogen flow. The synthesis of PbSe/CdSe HNCs was performed in a nitrogen-filled glovebox. Both the storage of samples and their manipulation for structural and optical characterization were performed in a glovebox under nitrogen atmosphere in order to avoid post-synthesis oxidation.

Synthesis of PbSe Cores with Different Shapes. PbSe NCs with different shapes have been synthesized by published procedures with slight modifications.[16,17] The synthesis of all PbSe NCs were carried out in a standard Schlenk line in nitrogen atmosphere. For the synthesis of cubic PbSe NCs, 1.7 mmol of lead acetate trihydrate (99.999% Aldrich), 1.5 mL of oleic acid (OLAC, 90% Aldrich), 8 mL of trioctylphosphine (TOP, 90% Fluka), and 2 mL of diphenylether (DPE) were degassed under a vacuum (1×10^{-3} mbar) at 120 °C for about 2 h. This Pb-oleate solution was purged in nitrogen and cooled down to room temperature. The Pb-oleate solution was then mixed with 1.7 mL of a 1 M solution of Se (99.999% Alfa Aesar) in TOP. This mixture was fast injected in a flask containing 10 mL DPE purged under nitrogen atmosphere at 190 °C. The reaction mixture was kept at 155 °C for 20 min and finally fast quenched with the injection of a 1:2 mixture of methanol/butanol. The mixture was finally purified by two cycles of precipitation in methanol, centrifugation, and redispersion in toluene. This procedure of quenching and purification of the particles was adopted for all types of PbSe NCs.

The growth of star-shaped PbSe NCs was obtained with the same synthesis procedure but in presence of small amounts of acetate (Pb:Acetate ~5:1). In this synthesis, Pb-precursor was dried at 80 °C for about 30 min, hence small amounts of acetate are still present in the solution. After the injection, the flask was kept at a temperature of 140 °C for 10 min.

For the synthesis of PbSe nanorods, 13 mL of DPE were degassed under a vacuum for about 30 min at 120 °C and successively heated up under nitrogen flow up to 240 °C. At this temperature 9 mL of Pb-oleate precursor were injected and the temperature was stabilized at 190 °C. After short aging, 0.6 mL of the Se-precursor (1 M in TOP) were injected and the heating source was shortly removed in order to allow a fast temperature drop to 140 °C. The reaction was allowed to proceed at this constant temperature for 20 min and finally quenched by fast injecting a mixture of methanol and butanol. Two other cycles of purification (alcohol-induced precipitation and solubilization in toluene) were necessary in order to remove the excess of surfactants. We remark that this synthesis procedure is strongly affected by the concentration of precursors and by the temperature stabilization speed, which may influence the shape and faceting of the first nanocrystalline nuclei formed. By quenching the reaction at about one minute after injection, particles are isolated that are partly attached. This experimental evidence points to the occurrence of an oriented-attachment mechanism, accordingly with previous published papers on anisotropic PbSe.[14,15] Other factors may also play an important role in the reaction kinetics, like the formation of Pb-carboxylate complexes after Pb-oleate injection.

Synthesis of PbSe/CdSe Core/Shell HNCs. We studied Cd^{2+}-for-Pb^{2+} CE starting from PbSe NCs with different shapes. CE was achieved by a dropwise injection of a Cd-oleate precursor in a reaction flask containing a solution of PbSe NC seeds, according to the procedure published by Pietryga et al. with some modifications.[8] Particles were isolated at different reaction times, from 10 min up to several hours, and were analyzed by HRTEM, EDX (see the Supporting Information, S2), and HAADF-STEM in order to identify which facets of PbSe were attacked first and to verify the progression of CE and structure transformation over time. The used HAADF-STEM technique combines the atomic resolution of the STEM technique with Z-contrast and, therefore, provides also compositional information. Hence it allows us to study the atomic structure and chemistry of the formed heterointerfaces.

For the preparation of the Cd-precursor, we dissolved 2.2 mmol of cadmium acetate hydrate (99.99% Aldrich) in 2 mL of oleic acid (OLAC, 90% Aldrich) and 4.3 mL of diphenylether (DPE, 99% Aldrich) and degassed under vacuum at 120° for about 2 h. This precursor was then stored in nitrogen atmosphere and heated up to 100 °C. A solution of PbSe NCs (about 10 mg nanoparticles, corresponding to approximately 1/3 of the synthesized batch) in 5 mL octadecene (ODE, 98% Aldrich) was prepared in a nitrogen-filled glovebox and heated up to 100 °C (T_{inj}). Once the temperature was stabilized to this value, 2 mL of the Cd-precursor solution (containing 0.7 mmol of Cd), were injected dropwise in about 1 min via a glass pipet. In a first set of experiments, after this first injection, the temperature was kept constant at 100 °C and multiple injections of additional Cd-oleate precursor, 0.25 mL at a time, were performed at regular intervals of about 2 h over a total 12 h time. By sampling at the end of every stage (before each additional injection) we isolated particles at different stages and analyzed them by TEM, HRTEM, absorption/photoluminescence spectroscopy. This control experiment showed no significant change in the particles structure and properties over time when the temperature is kept constantly at 100 °C over the whole synthesis.

To achieve a progressive CE, from partial to complete Pb to Cd conversion, we performed a stepwise programmed increase in temperature in the 100−200 °C range. Each temperature increase step was followed by the dropwise injection of additional Cd-precursor in order to ensure a constantly high precursor concentration in solution. In these experiments, the ~10 mg of PbSe NCs were dispersed in 5 mL of ODE and heated up to 100 °C. Two milliliters of Cd-precursor solution (containing 0.7 mmol of Cd), were then injected dropwise in about 1 min via a glass pipet and the reaction was allowed to proceed for about 2 h. The temperature was then increased up to 130 °C and 0.25 mL of Cd-precursor was injected in order to ensure a constantly high concentration of Cd in solution. The reaction was allowed to proceed at this temperature for about 1 h and about 0.3 mL of solution were sampled (stage T2). In a third step, a further increase in temperature was performed up to 150 °C, 0.25 mL of Cd-precursor were injected and the reaction was carried out at this temperature for an additional hour (stage T3). A complete conversion of PbSe to CdSe NCs was achieved by performing an additional step in which the temperature was increased in the 170−220 °C range, 2 mL of Cd-precursor were injected dropwise and the system was allowed to grow for 2 h (stage T4). The reaction was finally quenched by removing the heating source and the mixture was allowed to cool down to room temperature. Experimental details are summarized in Table 1. We remark here that for rod-shaped NCs a temperature as high as 190−200 °C is sufficiently high to allow a complete conversion of PbSe to CdSe, while a slightly higher temperature of 210−220 °C is needed for NCs with a considerably higher volume, like the cubic and star-shaped NCs described above. The reaction was finally quenched by removing the heating source and the mixture was allowed to cool down to room temperature. After the synthesis, 2 mL of hexane were

dx.doi.org/10.1021/cm202796s | Chem. Mater. 2012, 24, 294−302

Table 1. Experimental Details for the Synthesis of PbSe/CdSe HNCs at Different Reaction Stages

reaction time (min)	operation	temperature (°C)	stage
0	injection 2 mL	100	T0
120	sampling T1	100	T1
125	injection 0.25 mL	130	
180	sampling T2	130	T2
185	injection 0.25 mL	150	
240	sampling T3	150	T3
245	injection 2 mL	200	
360	sampling T4	200	T4

added to the reaction mixture. The extraction/purification procedures of the HNCs were carried out in a glovebox by performing two cycles of alcohol-induced precipitation (by addition of a methanol/butanol mixture) and redissolution in toluene. In this set of experiments, a small amount of HNCs solution was sampled by withdrawing at the end of every growth stage (named T1–T4). After purification, the particles were analyzed by different techniques, like TEM, HRTEM, HAADF-STEM, and absorption/PL spectroscopy. We remark that we also performed another set of experiments in which the synthesis was quenched at the end of each of the four stages of CE and the particles were purified with the same procedure described above and analyzed with the same techniques. These experiments indicate that samples isolated at the same reaction stages show the same structure and features, independently on the sampling method.

A control experiment was performed to verify whether a complete conversion of PbSe to CdSe is feasible at a temperature of 150 °C by increasing the amount of injected Cd precursor. CE was performed from PbSe NCs of different shapes in the same conditions described above, up to stage T3. After the injection at 150 °C, the temperature was kept constant for 2 h. Successively, other injections of 0.25 mL each were performed every 2 h in overall 8 h. The obtained particles, after purification from unreacted species, were analyzed by HRTEM, showing that PbSe cores are still present in the HNCs.

RESULTS

The first system studied consists of cubic NCs, which represents the most stable shape of rs-PbSe. Because of its crystallographic simplicity and mixed Pb–Se facets, it serves as a model system for the study of the PbSe-CdSe heterointerface evolution. The formation of cubic rs- PbSe NCs is promoted by increasing the reaction time and temperature, leading to thermodynamically stable cubes with (100) facets (Figure 1a). Figure 1 shows an overview of cubic PbSe NCs before (Figure 1a) and after progressive stages of CE (Figure 1b–d). It can be immediately observed that the particles preserve their overall size (see the Supporting Information, S3) and shape at the different reaction stages, whereas two distinct crystalline sections form. The HAADF-STEM image in Figure 1b shows a HNC formed at an early reaction stage (stage T1 of CE). The picture clearly displays the formation of a crystalline section with a lower contrast compared to PbSe, and which structure is consistent with that of zb-CdSe. The presence of CdSe is furthermore confirmed by EDX analyses, which also exclude the presence of elements different from Cd, Pb and Se (see the Supporting Information, S2). Hence, CE is starting selectively at the (truncated) corners of the PbSe cubes. It was found that at a reaction temperature of 100 °C neither an increase in reaction time up to 12 h, nor an increase in the Cd-precursor concentration produce any remarkable increase in the shell thickness (see the Supporting Information, S4a).

In contrast, CE proceeds further by progressively increasing the reaction temperature from 100 to 200 °C in a stepwise

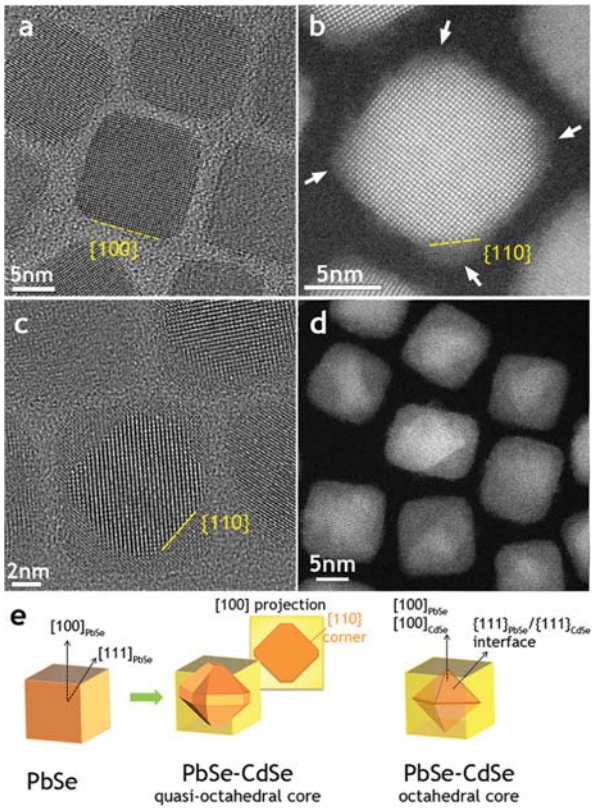

Figure 1. (a) HRTEM image of cube-shaped PbSe NCs in the [100] zone axis. (b, d) HAADF-STEM and (c) HRTEM images of PbSe/CdSe HNCs with progressing degree of CE from b to d. Small CdSe NC-sections in b are emphasized by white arrows. (e) Sketch of the structural transformation from pure PbSe cube-shaped NCs (left) to core–shell PbSe/CdSe HNCs with a nearly octahedron PbSe core. The PbSe is indicated in orange, CdSe in yellow.

manner (see the Supporting Information, S1). Images c and d in Figure 1 show illustrative HRTEM/HAADF-STEM pictures of the HNCs obtained at two progressive steps of CE, at 130 °C (stage T2) and 150 °C (stage T3), respectively. The formed HNCs consist of quasi-octahedral PbSe cores embedded in a CdSe matrix with sharp interfaces. We observe approximately octahedral PbSe cores as a "diamond" shape in the [100] viewing direction, with atomically sharp {110} edges (a scheme of the interfaces and their displacement in three dimensions is given in Figure 1e). We can conclude that at every reaction step CE does not proceed isotropically, but rather preferentially in the ⟨111⟩ direction with the formation of sharp $\{111\}_{PbSe}$/$\{111\}_{CdSe}$ interfaces.

A second structural study was carried out on colloidal PbSe nanocrystals with a star-shape, which display branches in the six ⟨100⟩ directions (Figure 2a). These PbSe NCs form by oriented attachment of small particles along the [100] crystal axis, which is triggered by small amounts of acetate in solution.[16]

Compared to cubic particles, star-shaped PbSe NCs have more high-index facets exposed to Cd-precursor in solution; these facets may have a different propensity toward CE. Figure 2 shows an overview of star-shaped particles isolated at the progressive stages (increased reaction time and temperature) of CE (see the Supporting Information, S1). A comparison between star-shaped PbSe (Figure 2a) and PbSe-CdSe (Figure 2b) particles in the same [100] zone axis, shows that after CE a

dx.doi.org/10.1021/cm202796s | Chem. Mater. 2012, 24, 294–302

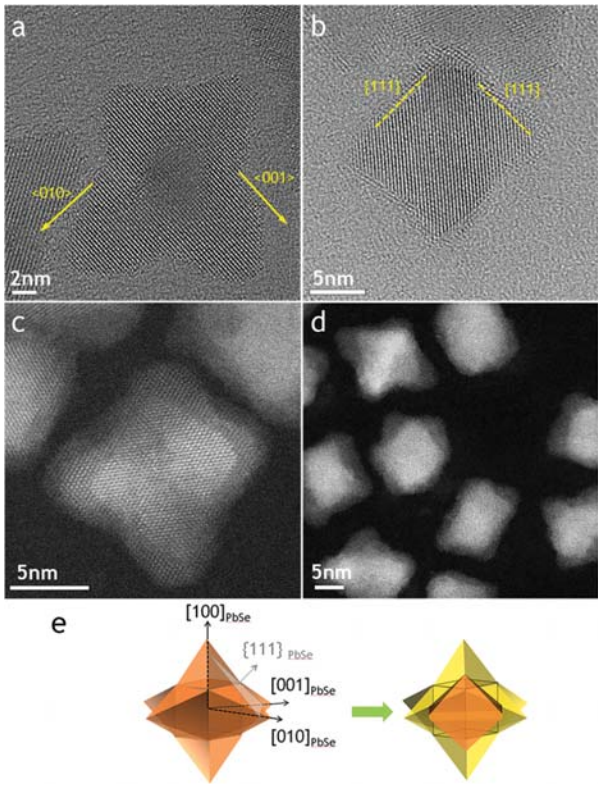

Figure 2. HRTEM images of (a) star-shaped PbSe NCs before CE (in the [001] zone axis), and (b) at the first stage of CE (in the [1−10] zone axis). (c, d) HAADF-STEM of PbSe-CdSe HNCs after advanced CE. (e) Sketch illustrating facets displacement in PbSe and PbSe-CdSe HNCs in the [100] zone axis. The PbSe is indicated in orange, CdSe in yellow.

thin shell of CdSe forms, with preservation of the overall shape and with the dominant occurrence of sharp {111} interfaces between the shell and the octahedral-PbSe core (Figure 2b−d). The displacement of the CdSe/PbSe interfaces in the [100] zone axis is presented in the illustrative sketch in Figure 2e. Increased reaction time and temperature lead to the formation of a progressively thicker shell (Figure 2d), through the formation of {111}-faceted PbSe cores and up to a complete conversion of PbSe to CdSe (see the Supporting Information, S4d). We note that complete CE allows growing zb-CdSe NCs with yet unseen "unnatural" shapes, such as cubic and near-octahedral star shapes (see the Supporting Information, S4c,d).

Interesting results have been achieved by studying CE in PbSe nanorods oriented along the [100] direction. It has been already demonstrated that PbSe NRs and nanowires can form in solution by oriented-attachment of PbSe quasi-spherical particles in the [100] direction and their successive ripening.[18,19] We observed the formation of rod-shaped particles in particular conditions of precursor concentration and temperature that may promote an efficient time-separation of the nucleation and successive attachment/growth of the PbSe NCs. The resulting particles were monocrystalline rs-PbSe with preferential [100] axis along the length of the rod (Figure 3a), with average diameter of 6 nm and length of 20 nm (see the Supporting Information, S2). For simplicity, PbSe NRs can be represented as attached cubes sharing {100}-type facets (first step of Figure 3g).

At an early reaction stage (stage T1 of CE, 100 °C, 2 h) a thin shell of CdSe can be detected at the surface of the NRs. The HRTEM insight presented in Figure 3b−c shows that the PbSe cores preserve the rs-structure with the preferential ⟨100⟩ long axis, whereas a thin zb-CdSe shell is present at the surface. Particles observed in different zone axes (e g. in the [001] and [110] projections in images b and c in Figure 3, respectively) show the formation of sharp {111} and {100} interfaces. In all projections, it is evident that the formed CdSe shell is not homogeneous, but rather thicker in the ⟨111⟩ direction. This effect is observable not only at the NR tips, but also in correspondence of the NR sidewalls, which are strongly {111}-faceted (Figure 3c). This feature is even more evident in advanced stages of CE (stage T2 of CE, 130°, 3 h), where an increase in the shell thickness is accomplished. From the HAADF-STEM overview in Figure 3d−f we gather that at this reaction stage the HNCs consist of core−shell NRs, where the PbSe inner rod has adopted a zigzag shape terminated by {111} interfaces. We remark that at this reaction stage a few particles present an octahedral core (top particle in panel f).

Further on (stage T3 of CE, 150°, 4 h), anisotropic CE leads to {111}-faceted quantum dot cores of rs-PbSe embedded in a zb-CdSe NR. The lower-resolution sample overview is given by the HAADF-STEM image in Figure 4a, in which PbSe cores can be easily distinguished from the CdSe rod-shell due to the higher contrast. Interestingly, the PbSe core is mostly located at the center of the NR and there are some rods in which two PbSe dots are clearly observed, as shown in the HRTEM picture in Figure 4c. A picture of the HNC structure with atomic resolution is given by Figure 4b, showing the phase image of a reconstructed exit wave, obtained from a through-focus series of HRTEM images. Zb-CdSe NRs are formed with the [100] zb-CdSe axis along the length of the rod, while the rs-PbSe is in a cube-to-cube orientation with the cubic CdSe; the cores are strongly faceted with dominating {111} interfaces. Stacking faults in the CdSe are commonly observed, often starting at the edges of the core, as indicated by the arrow in Figure 4b. It is worth noting that such planar defects were never observed in pure PbSe NCs, whereas they have been often detected in their HNC counterparts in advanced stages of the Pb^{2+} to Cd^{2+} conversion (Figure 4b).

Finally, after successive CE stages, pure CdSe NRs can be obtained, which have the zb-crystal structure (Figure 4d). The synthesis of wurtzite CdSe NRs is common practice, as the growth of the polar {0001} surface can easily be promoted under wet chemical conditions.[20] However, zb-CdSe NRs are very uncommon, and the procedures used here provide a new route to the synthesis of zb-CdSe rods.

A preliminary study shows that these rod-shaped PbSe-CdSe HNCs obtained by CE show bright and stable photoluminescence in the near-infrared with a PL lifetime in the microsecond range. Absorption spectra of pure PbSe NRs and core/shell PbSe/CdSe NRs are presented in Figure 4f, showing that the formation of a CdSe shell causes a blue-shift of the first- excitonic absorption peak, due to the shrinking of the PbSe NR core. Emission spectra of pure PbSe NRs are not reported, since the PL energy falls out of the range of the available IR detectors. Figure 4g shows the PL spectra of PbSe/CdSe NRs at three progressive stages of CE process (from stage T1 to T3). It can be observed that by increasing the extent of the CE, particles are obtained whose bright PL is considerably shifted toward higher energies, in agreement with the progressive shrinking of the PbSe NR core (see also Table S6 in the Supporting Information). The results presented above show that CE is a valuable approach to obtain PbSe NRs with a

dx.doi.org/10.1021/cm202796s | Chem. Mater. 2012, 24, 294−302

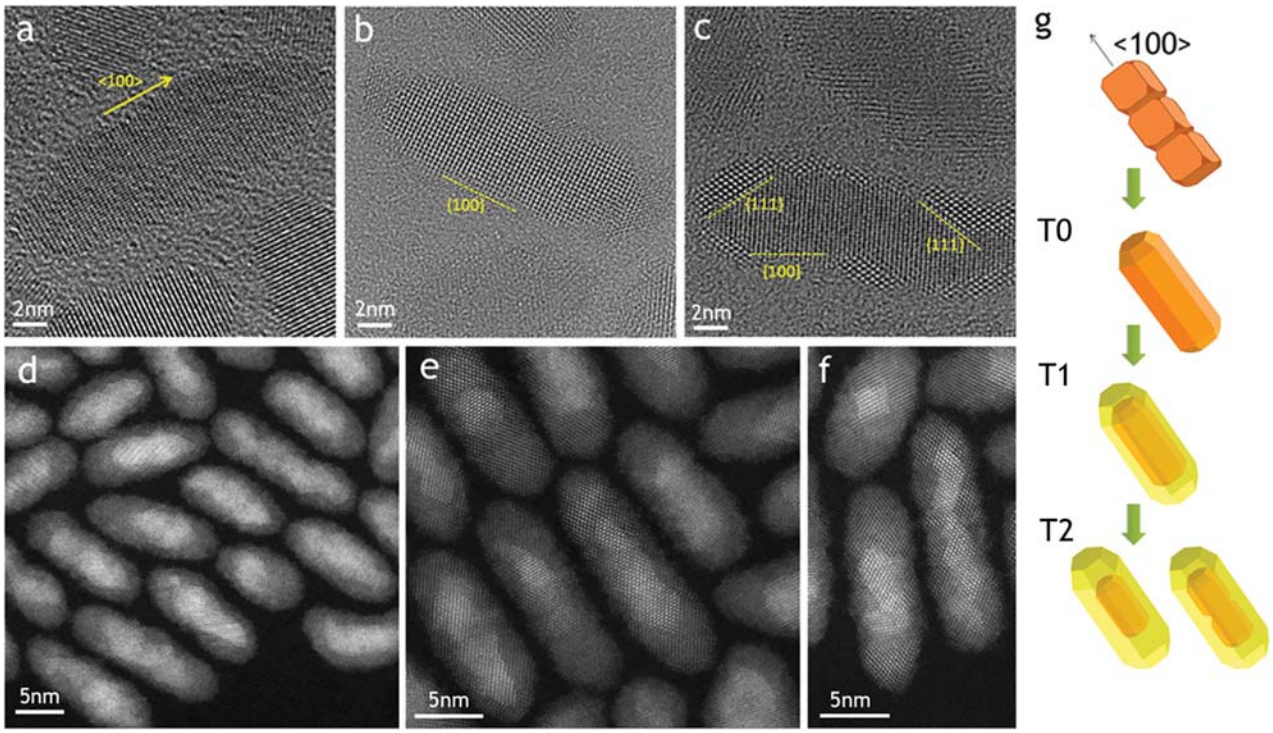

Figure 3. HRTEM image of rod-shaped PbSe NCs (a) before CE (T0), in the [110] zone axis, and (b, c) at the first stage of CE (T1), observed (b) in the [001] zone axis and (c) in the [110] zone axis. (d–f) HAADF-STEM pictures of NRs in the second stage of CE (T2): PbSe cores can be distinguished from the CdSe shell due to the different contrast. (g) Sketch illustrating the formation of PbSe NRs and their progressive conversion to core–shell PbSe/CdSe HNCs. The PbSe is indicated in orange, CdSe in yellow.

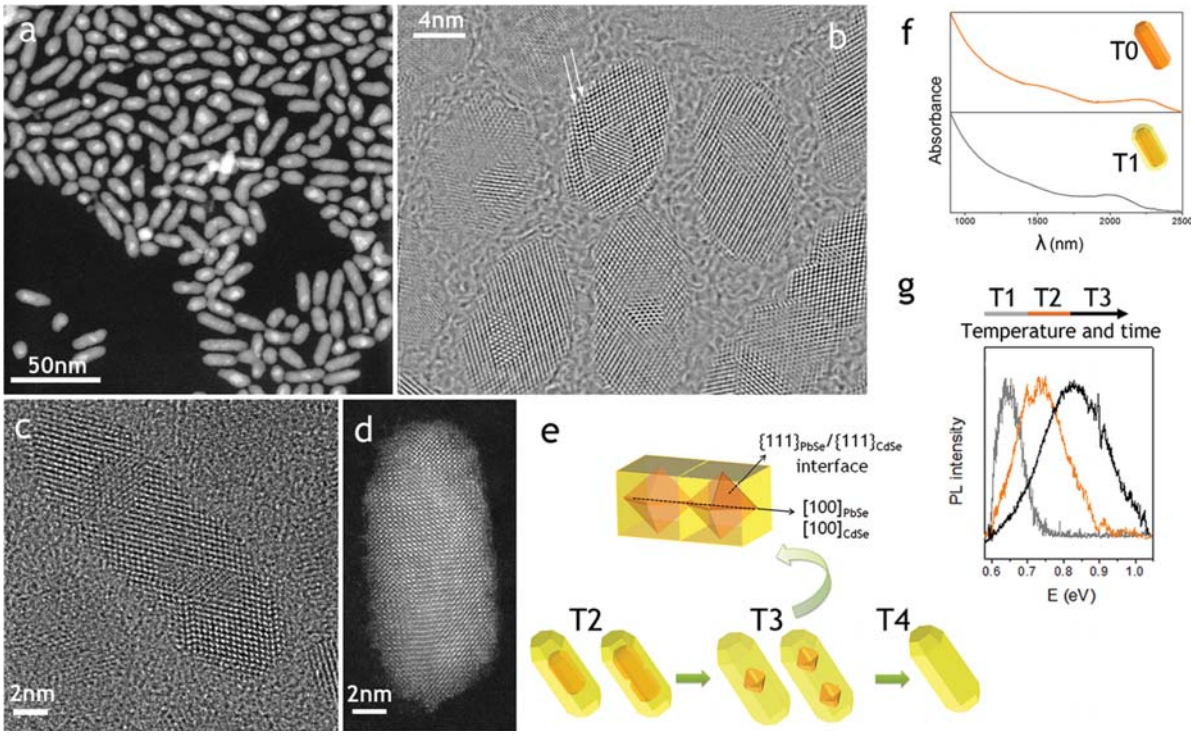

Figure 4. (a) HAADF-STEM image of PbSe/CdSe core/shell NCs with dot-in-a-rod structure obtained after CE at 150 °C (T3). Aberration-corrected HRTEM images of (b) one or (c) two rs-PbSe dots are embedded in a zb-CdSe rod-shaped matrix. (d) HAADF-STEM image of a pure zb-CdSe NR obtained after complete CE from PbSe NRs (T4). (e) Sketch of the formation of one or two octahedral PbSe dots in a CdSe NR-shell from core–shell PbSe/CdSe NRs with {111} faceting at the interface. (f) Normalized absorption spectra of PbSe NRs (T0) and core–shell PbSe/CdSe NRs (T1); (g) normalized PL spectra of PbSe/CdSe HNCs at the different stages of CE; black, orange and gray peaks correspond to the PL spectra of samples obtained at first, second and third stage of CE (T1–T3), respectively.

dx.doi.org/10.1021/cm202796s | *Chem. Mater.* 2012, 24, 294–302

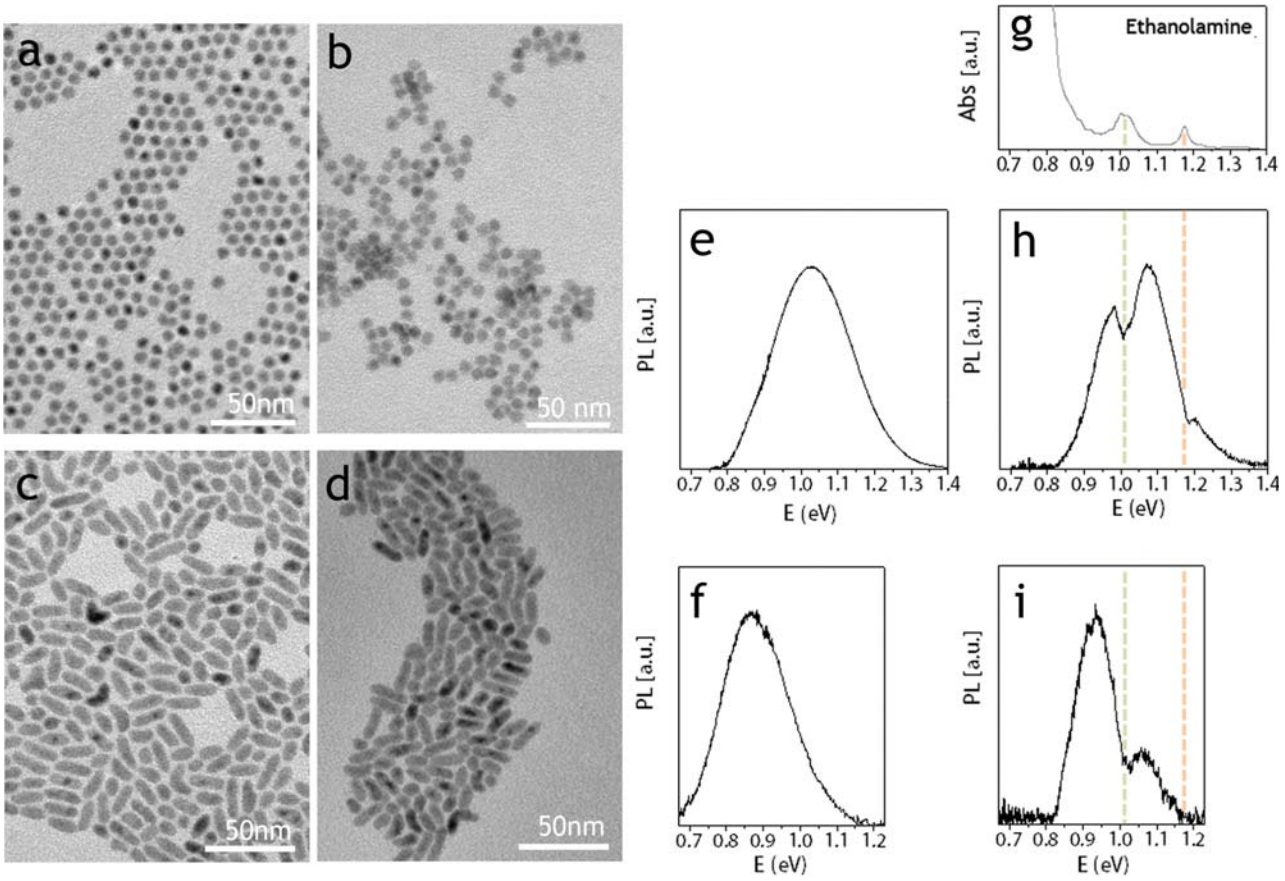

Figure 5. (a–d) TEM images of HNCs before (left) and after (right) the ligand exchange with $Sn_2Se_6^{4-}$. The HNCs consist of PbSe cores embedded in a thick shell of CdSe with spherical (a, b) and rod- (c, d) shape, respectively. (e, f) Photoluminescence spectra of the PbSe/CdSe HNCs capped with oleate and soluble in tetrachloroethylene; the HNCs have a spherical and a rod- shape, respectively. (g) Absorption spectrum of ethanolamine (solvent). (h, i) Photoluminescence spectra of the PbSe/CdSe HNCs capped with tin chalcogenide and dispersed in ethanolamine; the HNCs have a spherical and a rod shape, respectively.

tunable emission in the near-IR region, since the synthesis of pure PbSe NRs with controlled geometrical parameters is still difficult to achieve in a single step.[11,19] It deserves consideration that rod-shaped semiconductor NCs have a high potential for linearly polarized emission.[21,22] In this respect, the CE-synthesis of NRs with dot- and rod-shaped PbSe cores and CdSe shell could be a strategy to achieve emitters of polarized light in the IR, because the CdSe rod shell may induce a polarization of the PbSe core emission.

These properties make PbSe/CdSe HNCs of great interest for the realization of opto-electronic devices, like photon detectors an photovoltaic cells. One of the limits for the implementation of NCs in opto-electronic devices is the presence of an insulating shell of organic capping at the NC surface. Recently, different strategies have been developed to successfully replace organic capping from the surface of colloidal NCs of several materials with all-inorganic ligands.[23−25] The advantage of using such conductive inorganic ligands consists in increasing short-range interparticle communication and thus extending the processability of the NCs. For this purpose, a ligand exchange procedure has been applied to PbSe/CdSe HNCs in order to replace organic surfactants with a metal chalcogenide in hydrazine ($(N_2H_4)_3$ $(N_2H_5^+)_4$ $Sn_2Se_6^{4-}$) and consequently transfer the particles to polar solvents (more experimental details are reported in the Supporting Information).[23] We remark that hydrazine is a toxic chemical which must be handled with appropriate protective equipment. Particles with different shapes and shell thickness have been studied. Here we present the study of two representative types of HNCs, with spherical and rod shape, respectively, characterized by the presence of a thick shell of CdSe (more than 1 nm on average). The particles shown in Figure 5a-b are spherical HNCs of 7.8 (± 0.6) nm diameter consisting of PbSe cores of about 2.5 (± 0.5) nm embedded in a CdSe shell; these particles have been obtained from spherical PbSe NCs[17] by CE according to the procedure described in the Experimental Section (stage T2 of CE). In a similar way, rod-shaped HNCs with a PbSe core of 3.5 (± 1) nm (Figure 5c,d) have been obtained by CE from PbSe NRs (stage T3 of CE). TEM pictures of the PbSe/CdSe HNCs, before (left) and after (right) ligand exchange with tin chalcogenide, are shown in Figure 5. After ligand exchange the particles preserve their size and shape, they are stable in the polar solvent (ethanolamine) and no aggregation is observed at TEM. Figure 5e, f, h, i displays the photoluminescence spectra of spherical and rod-shaped core/shell PbSe/CdSe HNCs before (left) and after (right) ligand exchange. Before ligand exchange the particles are capped by oleic acid and dissolved in tetrachloroethylene, whereas after ligand exchange they are functionalized with $Sn_2Se_6^{4-}$ and dispersed in ethanolamine.

By comparing the PL of these core/shell particles before (Figure 5e, f) and after (Figure 5h, i) the ligand exchange, it is

dx.doi.org/10.1021/cm202796s | Chem. Mater. 2012, 24, 294–302

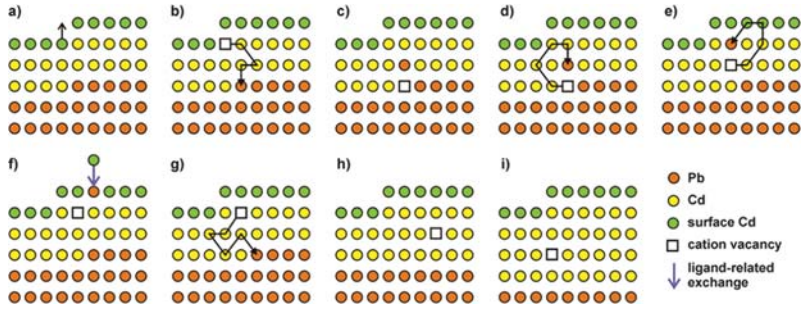

Figure 6. Schematic of a plausible mechanism for cation exchange in a two-dimensional projection of the HNC interface. The sketch shows Pb (orange) and Cd (yellow) atom positions in the PbSe-CdSe HNC lattice at the {111} interface. Light green dots represent surface Cd atoms; Se anions are not shown. (a) The formation of a cation vacancy at the surface is followed by (b) diffusion of the vacancy to the PbSe/CdSe interface. (c–e) Next, the Pb atom can diffuse to the interface by means of vacancy-assisted migration, whereby many (Cd-associated) vacancy jumps are required to enable (f) diffusion of Pb to the surface, where it undergoes a ligand-enabled Cd-for-Pb exchange. (b–g) This process continues until (h) the {111}Pb layer is completely replaced by Cd atoms, after which (i) the next Pb layer is replaced. (b, d, e, g) only one of many possible vacancy diffusion paths is shown.

clear that HNCs capped with $Sn_2Se_6^{4-}$ preserve their luminescence in the near IR. After the ligand exchange the HNCs become soluble in some polar solvents, for example they are very stable in hydrazine or ethanolamine. Unfortunately, these solvents also absorb light in the 1200–1700 nm range of interest and a partial absorption by the solvent is observed in the samples. As a result, measurement of the exact photoluminescence quantum yield is difficult to achieve. We measured a photoluminescence quantum yield of about 3%, which can be accounted as the "minimum" quantum yield of PbSe/CdSe HNCs in ethanolamine, capped with $Sn_2Se_6^{4-}$.

We remark that the stability of the particles is affected by the thickness of the CdSe shell. The results presented in Figure 5 concern particles consisting of PbSe cores with a thick CdSe shell. Conversely, HNCs with a shell of CdSe thinner than ~0.8 nm, on average, are less stable over time and the formation of a precipitate in the HNC dispersion can be observed after a few days. It is worth noting that this ligand exchange procedure can also be applied to pure PbSe NCs, but the strong interparticle interactions cause most of the particles to undergo uncontrolled aggregation. The growth of a CdSe shell on PbSe NCs shows up to be a successful strategy to improve surface stabilization and the processability of PbSe NCs, whereas preserving their individual opto-electronic properties.

DISCUSSION

From the results presented above, it appears that Cd^{2+}-for-Pb^{2+} CE in a native PbSe rs-lattice is a temperature-activated anisotropic process. From the HRTEM study it is clear that the Se sublattice remains essentially coherent across the interface and the structural transformation proceeds mainly through the cation sublattice. The conditions for CE are moderate temperatures (100–200 °C) and constantly high overall Cd-precursor concentrations, with a ratio of Pb (contained in the NCs) to Cd precursor in solution of about 1:20–1:50. Under these conditions, the mass flow from the solution to the NC surface is sufficiently high not to be rate-limiting. We also note that the percentage of Cd contained in the NC at the individual reaction stages, i.e., at a given temperature, is comparable for samples with comparable volume but different shapes, and consequently different facets exposed (see the Supporting Information, S1 and S2). This excludes that the CE is triggered by the selective adsorption of the Cd-precursor at specific facets, which is instead the limiting step for the diffusion of impurities in doped NCs.[26]

Another striking experimental evidence is that CE is strongly anisotropic. The {111} PbSe/CdSe interfaces are clearly dominating, hence ion exchange appears to be most effective in creating this specific crystallographic plane. In that respect, the strong {111}-faceting observed in all types of PbSe-CdSe HNCs, regardless of the shape, is noteworthy. The dominant formation of {111}-interfaces also causes the PbSe inner rod to be {111}-faceted so that it adopts a zigzag shape (Figure 3c–f), which may further facilitate the formation of an octahedral core and, occasionally, the breaking up into multiple cores (Figure 4c, e). Anisotropic CE in specific crystallographic directions has been already observed in other nanocrystalline systems, like wurtzite- CdS/chalcocite- Cu_2S with rod and octapod shape.[12,27] In these systems CE starts preferentially at the tip regions of the pods and progresses toward the core with the formation of specific interfaces which are energetically favored. It was found that these specific interfaces have a lower activation barrier and a lower lattice mismatch.[12,27] Similarly, the selective formation of {111} interfaces between rs-PbSe and zb-CdSe HNCs could be energetically less demanding. Nevertheless, the anisotropic CE in PbSe-CdSe cannot be explained in terms of a strain-driven process, since the variation of lattice mismatch at the different zb-CdSe/rs-PbSe interfaces is not significant (less than 1%).[8] Although the lattice parameters are nearly identical, the two materials show different crystal structures (with 6-fold coordination for the rs lattice and 4-fold coordination for the zb one). The cation and anion sublattices (Cd, Pb, and Se) are very similar, though, since they all have the face-centered-cubic (fcc) crystal structure. One feature that makes the {111} interface different from other low-index interfaces (such as {001} and {110}), is that it consists entirely of either cations or anions. In the ideal case, the interfacial Se{111} atomic layer is flanked by a Pb{111} layer at one side, and by a Cd{111} layer at the other side, providing a very neat, stress-free interface, as confirmed by density functional theory (DFT) calculations.[28] The question is now how the cation exchange proceeds kinetically at the atomistic level. A schematic of a plausible mechanism is shown in Figure 6, where it is presumed that the solid diffusion of Cd, Pb atoms within the nanostructure takes place through vacancy-assisted migration[29,30] in the cation sublattice.

Vacancies are often present in compound nanostructures that are synthesized under wet chemical conditions, as their composition is never perfectly stoichiometric. Furthermore, cation exchange is a very powerful and invasive process that is likely able to generate vacancies due to the strong chemical potentials applied (we remark here that cation exchange even leads to stacking fault generation, which requires much more energy than the formation of a single vacancy). In Figure 6, we presume that the vacancy is formed at the surface (a), after which it diffuses through the CdSe shell to the PbSe/CdSe interface (b). Please note that migration of vacancies means that atoms (Cd cations, in this case) jump into the vacancy, after which the vacancy occupies the lattice site left by the atom. Next, a Pb atom can jump into the vacancy, thereby leaving the PbSe core and entering the CdSe shell (c). Then, through multiple vacancy-assisted jumps that are stochastic in nature,[29] the Pb atom can reach the surface of the CdSe shell (d, e), after which it is exchanged for a Cd atom (f).

Figure 6b–g shows the cation exchange of the 'corner' Pb atom in a {111} atomic layer that consists only partially of Pb atoms. It is well-known that at free crystal surfaces, adatoms, corner atoms, and atoms at terrace steps have higher formation energy than regular surface atoms in a perfect surface. The same is true for atoms at interfaces: because the PbSe rs and CdSe zb structures have different atomic coordination, the interfacial 'corner' Pb atoms in the incomplete Pb/Cd atomic plane are in an energetically unfavorable position. Consequently, the removal of such a Pb atom requires much less energy than the removal of a Pb atom from a continuous atomic plane. Therefore, the {111}Pb atomic layer will be stripped atom by atom, until it is completely replaced with Cd atoms (Figure 6h). Eventually though, the following {111}Pb layer will also be exchanged for Cd (Figure 6i). A favorable nucleation site to 'break up' the next Pb layer could be at the intersection of two {111} interfacial facets. The exchange of incomplete layers will be fast in comparison to the 'breaking up' of the next Pb layer, which is why strong {111} faceting is apparent in all (S)TEM images (Figures 1–4), even though the cation exchange is halted at a random moment in time. HAADF-STEM tomography has confirmed that Pb/Cd intermixing only occurs at the PbSe/CdSe interfacial layer,[28] which is consistent with the atomistic model presented here.

Therefore, the anisotropy of the cation exchange process is most likely driven by the favorability of the {111}PbSe/{111}CdSe interface. We mention here that only this interface has a polar character, which possibly reduces the interface energy.

Here, we present a plausible mechanism. A full understanding of the energetics and kinetics of the anisotropic cation exchange will require extensive defect energy calculations (vacancy formation energies, activation energies for atomic jumps, solution energies, etc.), and simulations of CE in time (molecular dynamics simulations and/or kinetic Monte Carlo simulations to account for random nature of the vacancy jumping behavior). Although vacancy-assisted migration is a very plausible mechanism to explain the observations, it cannot be excluded that other mechanisms (interstitial cation diffusion, or favorable diffusion within the plane of the interface) play a role.

According to the proposed mechanism, CE is triggered by the formation of vacancies or interstitials, which concentration depends on the temperature as $[V, I] \approx \exp(-\Delta G_f/RT)$ (where [V, I] is the concentration of vacancies and interstitials and ΔG_f is the free energy for the formation of a vacancy or a vacancy-interstitial pair). The temperature-dependence of the rate of cation exchange could therefore be related to the density of cation vacancies that initiate the process. However, the formation of vacancy/vacancy-interstitial pairs is only one of the temperature-dependent processes involved. The structural reorganization of the rs lattice (6-fold coordination) into the zb lattice (4-fold coordination) is another process that may strongly depend on the temperature.

CONCLUSION

In conclusion,we have presented a study of Cd^{2+} for Pb^{2+} cation exchange from PbSe colloidal NCs with different geometries. A detailed structural study (by HRTEM/HAADF-STEM) has revealed that the CE proceeds dominantly in the ⟨111⟩ crystallographic direction, regardless of the area of the {111} facets in the starting PbSe NCs and is strongly temperature-dependent. This experimental evidence suggests that CE in the PbSe/CdSe HNC system proceeds through a temperature-activated layer-by-layer replacement of cations at the {111} NC interfacial facets, which can be plausibly explained by a vacancy-assisted cation diffusion mechanism. Interestingly, by performing sequential CE, new structures can be obtained, e.g., two-PbSe dots-in-a-CdSe rod HNCs. These nanomaterials may provide a novel platform for the study of electronic coupling between semiconductor quantum dots.

ASSOCIATED CONTENT

Supporting Information

Materials and methods, scheme for synthesis paths, compositional analysis by EDX, size-statistics, additional HRTEM pictures of PbSe/CdSe core/shell HNCs, ligand-exchange procedure for the transfer of the HNCs into polar solvents, correlation between PL and core size. This material is available free of charge via the Internet at http://pubs.acs.org.

AUTHOR INFORMATION

Corresponding Author

*E-mail: m.casavola@uu.nl; d.vanmaekelbergh@uu.nl.

ACKNOWLEDGMENTS

The authors acknowledge financial support from the European Union under the Seventh Framework Program (Reference EU-FP7 ITN Herodot) and under the Sixth Framework Program under a contract for an Integrated Infrastructure Initiative (Reference 026019 ESTEEM). DV thanks CW-NWO and FOM for financial support. The authors acknowledge Nico Hommels his contribution to the synthesis and Wiel Evers, Dr. C. A. van Walree and Prof. Dr. Celso de Mello-Donega for useful discussion.

REFERENCES

(1) Talapin, D. V.; Lee, J. S.; Kovalenko, M. V.; Shevchenko, E. V. *Chem. Rev.* **2010**, *110*, 389.
(2) de Mello-Donegá, C. *Chem. Soc. Rev.* **2011**, *40*, 1512.
(3) Reiss, P.; Bleuse, J.; Pron, A. *Nano Lett.* **2002**, *2*, 781.
(4) Wang, X.; Ren, X.; Kahen, K.; Hahn, M. A.; Rajeswaran, M.; Maccagnano-Zacher, S.; Silcox, J.; Cragg, G. E.; Efros, L.; Krauss, T. D. *Nature* **2009**, *459*, 686.
(5) Leitsmann, R.; Ramos, L. E.; Bechstedt, F.; Groiss, H.; Schäffler, F.; Heiss, W.; Koike, K.; Harada, H.; Yano, M. *New J. Phys.* **2006**, *8*, 317.

(6) Heiss, W.; Groiss, H.; Kaufmann, E.; Hesser, G.; Böberl, M.; Springholz, G.; Schäffler, F.; Koike, K.; Harada, H.; Yano, M. *Appl. Phys. Lett.* **2006**, *88*, 192109.
(7) Wald, F.; Rosenberg, A. J. *J. Phys. Chem. Sol.* **1965**, *26*, 1087.
(8) Pietryga, J. M.; Werder, D. J.; Williams, D. J.; Casson, J. L.; Schaller, R. D.; Klimov, V. I.; Hollingsworth, J. A. *J. Am. Chem. Soc.* **2008**, *130*, 4879.
(9) Lambert, K.; Geyter, B. D.; Moreels, I.; Hens, Z. *Chem. Mater.* **2009**, *21*, 778−780.
(10) Lee, D. C.; Robel, I.; Pietryga, J. M.; Klimov, V. I. *J. Am. Chem. Soc.* **2010**, *132*, 9960.
(11) Luther, J. M.; Zheng, H.; Sadtler, B.; Alivisatos, A. P. *J. Am. Chem. Soc.* **2009**, *131*, 16851.
(12) Sadtler, B.; Demchenko, D. O.; Zheng, H.; Hughes, S. M.; Merkle, M. G.; Dahmen, U.; Wang, L.-W.; Alivisatos, A. P. *J. Am. Chem. Soc.* **2009**, *131*, 5285.
(13) Son, D. H.; Hughes, S. M.; Yin, Y.; Alivisatos, A. P. *Science* **2004**, *306*, 1009.
(14) Jain, P. K.; Amirav, L.; Aloni, S.; Alivisatos, A. P. *J. Am. Chem. Soc.* **2010**, *132*, 9997.
(15) Robinson, R. D.; Sadtler, B.; Demchenko, D. O.; Erdonmez, C. K.; Wang, L.-W.; Alivisatos, A. P. *J. Am. Chem. Soc.* **2010**, *132*, 9997.
(16) Houtepen, A. J.; Koole, R.; Vanmaekelbergh, D.; Meeldijk, J.; Hickey, S. G. *J. Am. Chem. Soc.* **2006**, *128*, 6792.
(17) Wehrenberg, B. L.; Wang, C.; Guyot-Sionnest, P. *J. Phys. Chem. B* **2002**, *106*, 10634−10640.
(18) Cho, K. S.; Talapin, D. V.; Gaschler, W.; Murray, C. B. *J. Am. Chem. Soc.* **2005**, *127*, 7140.
(19) Koh, W.-k.; Bartnik, A. C.; Wise, F. W.; Murray, C. B. *J. Am. Chem. Soc.* **2010**, *132*, 3909.
(20) Manna, L.; Scher, E. C.; Alivisatos, A. P. *J. Am. Chem. Soc.* **2000**, *122*, 12700.
(21) Kazes, M.; Lewis, D. Y.; Ebenstein, Y.; Mokari, T.; Banin, U. *Adv. Mater.* **2002**, *14*, 317.
(22) Carbone, L.; Nobile, C.; et al. *Nano Lett.* **2007**, *7*, 2942.
(23) Kovalenko, M. V.; Scheele, M.; Talapin, D. V. *Science* **2009**, *324*, 1417.
(24) Nag, A.; Kovalenko, M. V.; Lee, J.-S.; Liu, W.; Spokoyny, B.; Talapin, D. V. *J. Am. Chem. Soc.* **2011**, *133*, 10612−10620.
(25) Kovalenko, M. V.; Bodnarchuk, M. I.; Zaumseil, J.; Lee, J.-S.; Talapin, D. V. *J. Am. Chem. Soc.* **2010**, *132*, 10085−10092.
(26) Erwin, S. C.; Zu, L. J.; Haftel, M. I.; Efros, A. L.; Kennedy, T. A.; Norris, D. J. *Nature* **2005**, *436*, 91.
(27) Miszta, K.; Dorfs, D.; Genovese, A.; Kim, M. R.; Manna, L. *ACS Nano* **2011**, *5*, 7176−7183.
(28) Bals, S.; Casavola, M.; van Huis, M. A.; Van Aert, S.; Batenburg, K. J.; Van Tendeloo, G.; Vanmaekelbergh, D. *Nano Lett.* **2011**, *11*, 3420.
(29) Simonovic, D.; Sluiter, M. H. F. *Phys. Rev. B* **2009**, *79*, 054304.
(30) van der Ven, A.; Ceder, G. *Phys. Rev. Lett.* **2005**, *94*, 045901.